

Supporting Information

A durable, scalable platform for the electrochemical conversion of CO₂ to formate; identifying pathways to higher energy efficiencies

Yingying Chen^a, Ashlee Vise^a, W. Ellis Klein^a, Firat C. Cetinbas^b, Deborah J. Myers^c, Wilson

A. Smith^{a,d,e}, Todd G. Deutsch^a, K.C. Neyerlin^{a*}

^a National Renewable Energy Laboratory, Golden, CO 80401, USA.

^b Energy Systems Division, Argonne National Laboratory, Lemont, IL 60439, USA

^c Chemical Sciences and Engineering Division, Argonne National Laboratory, Lemont, IL
60439, USA

^d Department of Chemical and Biological Engineering, University of Colorado Boulder,
Boulder, CO 80303

^e Renewable and Sustainable Energy Institute (RASEI), University of Colorado Boulder,
Boulder, CO 80303

**Corresponding Author: Kenneth.Neyerlin@nrel.gov*

Preparation of Cathode Catalyst Inks

The cathode catalyst inks were prepared by mixing commercial SnO₂ (< 100 nm, Sigma Aldrich) nanoparticles, Vulcan carbon (XC-72R, FuelCellStore), isopropanol alcohol (HPLC Plus grade 99.9%, Sigma Aldrich), deionized water (18 MΩ-cm), and ionomer (5 wt% Nafion ionomer (1100 EW, Ion Power) or 10 wt% PFAEM ionomer¹) together. The ratio of ionomer, catalyst, and Vulcan carbon was kept at 3:5:5. The solvent ratio of deionized water to isopropyl alcohol 2:3 was used. The ink concentrations of SnO₂ and Vulcan carbon ranged between 10-20 mg ml⁻¹ based on the target loading of the catalyst and the total surface area of the electrodes being prepared. The ink was first dispersed using a horn sonicator three times at 30 s intervals, and then the ink was placed in an ice bath sonicator for 1 hour to ensure uniform mixing before being deposited onto the gas diffusion layer (GDL).

Cathode GDE Fabrication

A GDL (Sigracet 39BC, FuelCellStore) with a thickness of 325 ± 25 μm was placed on a heated vacuum table at 95° C with the micro porous layer (MPL) facing up. The catalyst ink was hand-painted onto the GDL. The catalyst loading ranged between 0.1 mg cm⁻² and 1.5 mg cm⁻² and was verified by the weight difference of GDL before and after the hand painting. The actual catalyst loading is >85% of the target loading. Once fabricated, the cathode GDE was hot-annealed at 120 °C for 2 hours.

Electrochemical Cell Setup

A custom-built hardware with 25 cm² active area was used to evaluate the performance and durability of the electrochemical reduction of CO₂. A piece of Ni Foam (MFNi16m, MTI

Corporation) of 25 cm² with a thickness of 1.6 mm was placed against the anode flow field with triple serpentine flow channels (Figure S1) and was compressed to 91 % using 1.55 mm of polytetrafluoroethylene (PTFE) gaskets. Ni has repeatedly shown high stability and activity towards the oxygen evolution reaction (OER) in basic media.²⁻⁴ A commercial bipolar membrane (BPM) (FBM, Fumatech GmbH, FuelCellStore) was placed right next to the Ni foam in reverse-bias mode with the cation exchange layer (CEL) and the anion exchange layer (AEL) facing the cathode and anode, respectively. The BPM is composed of a sulfonated crosslinked poly-ether ether ketone (CEL) and a polysulfone with bicyclic amines (AEL), with a polyacrylic acid/polyvinyl pyridine salt complex in the junction between the CEL and AEL.⁵ A catholyte flow channel was created within the PTFE gasket measuring of 1.27 mm right next to the CEL of BPM . The catholyte flow channel was designed as a 'Z' shape in order to provide mechanical support to the BPM and cathode GDE with two 'fingers' (Figure S2). A gold wire (California Fine Wire Co.) of 25 μm thick and 125 μm wide was placed inside the catholyte flow channel on one of the 'fingers', 0.13 mm away from the cathode. This enabled the characterization of the potential drop through the cathode GDE in-operando. A cathode GDE with 25 cm² active area was placed against the cathode flow field sealed with PTFE gaskets and was compressed to 18% once the cell was tightened to 40 inch-pound. The endplates of the cell were heated to 60° C and kept constant for all experiments. The flow plates for cathode and anode were made from Ti and had a 25 cm² area of triple serpentine flow channels (Figure S1). CO₂ heated to 60° C was delivered to the cathode GDE through the cathode flow plate at a constant flow rate of 2 NLPM. 1 M potassium hydroxide (KOH) electrolyte made by dissolving KOH pellets (Certified ACS, VWR) in 18 MΩ cm deionized water was heated to 60 °C and fed to the anode flow plate at 50 mL min⁻¹. The 0.4 M potassium

sulfate (K_2SO_4) made by dissolving K_2SO_4 (ACS reagent 99.7% Sigma Aldrich) powder in $18\text{ M}\Omega\text{ cm}$ deionized water was fed to the catholyte layer at 40 mL min^{-1} .

A Gamry Reference 3000 Potentiostat with a Reference 30K Booster was used for the electrochemical measurements. Galvanodynamic polarizations were conducted from 0 to 500 mA cm^{-2} at a rate of $1\text{ mA cm}^{-2}\text{ s}^{-1}$. Different current densities were held for at least 60 s before liquid and gas product samples were taken and analyzed. A LabJack was connected to the Au wire and the cathode current collector to record the potential difference.

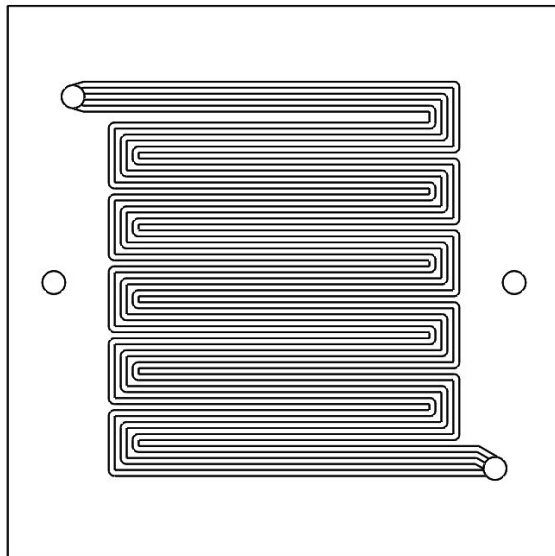


Figure S1 Pattern of the triple serpentine flow channels on the flow plates for anode and cathode.

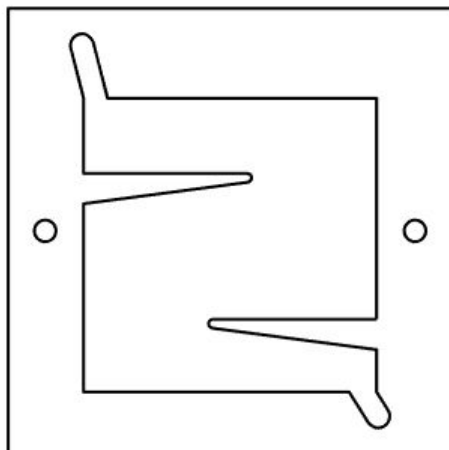


Figure S2 The 'Z' shaped flow channel for the catholyte buffer layer.

Product Quantitation

The effluent of the gas stream from the cathode flow plate and the liquid stream from the catholyte layer were mixed together and then separated using a gas trap. This ensured that all gas and liquid products were collected regardless of whether they exited from the catholyte channel of cathode flow plate. Liquid samples were collected for a given time (20 - 40 s) period, diluted to a known volume (25 – 100 mL) with 18 M Ω cm DI water, filtered with PTFE 0.22 μ m syringe filters into 2 mL vials. The vials with the liquid products were analyzed utilizing an Agilent 1260 Infinity II Bio-inert High-Performance Liquid Chromatography (HPLC) system. 20 μ L sample volume was injected into the HPLC via autosampler (G5668A) with 4 mM sulfuric acid (H₂SO₄) flowing at 0.6 mL/min (G5654A quaternary pump) as the mobile phase. The products in the samples were separated on a heated (35 °C, G7116A column thermostat) Aminex HPX-87H 300 x 7.8 mm Column (Bio-Rad) with a preceding Micro-Guard Cation H guard column. Formic acid was detected on a Diode Array Detector (DAD) at 210 nm with a bandwidth of 4 nm. The HPLC

chromatogram and the calibration curve of the formic acid standards are shown in Figure S3. The gas samples were analyzed in a 4900 Micro GC (10m, molecular sieve, Agilent) for at least three times. Samples were collected in Supel™ Inert Multi-Layer Foil Gas Sampling Bags (Sigma-Aldrich) for a recorded time (15 – 30 s) and manually inserted into the Micro GC for 100 μ s, within a maximum of 2 hrs after sampling. The injection temperature was set to 110 °C. Carbon monoxide (CO) and hydrogen (H₂) were separated within a heated (105 °C) and pressurized (28 psi) 10 m MS5A column with a carrier gas of argon (Matheson Gas- Matheson Purity). The compounds were detected on an integrated thermal conductivity detector (TCD). The GC chromatogram and calibration curves of CO and H₂ are shown in Figure S4.

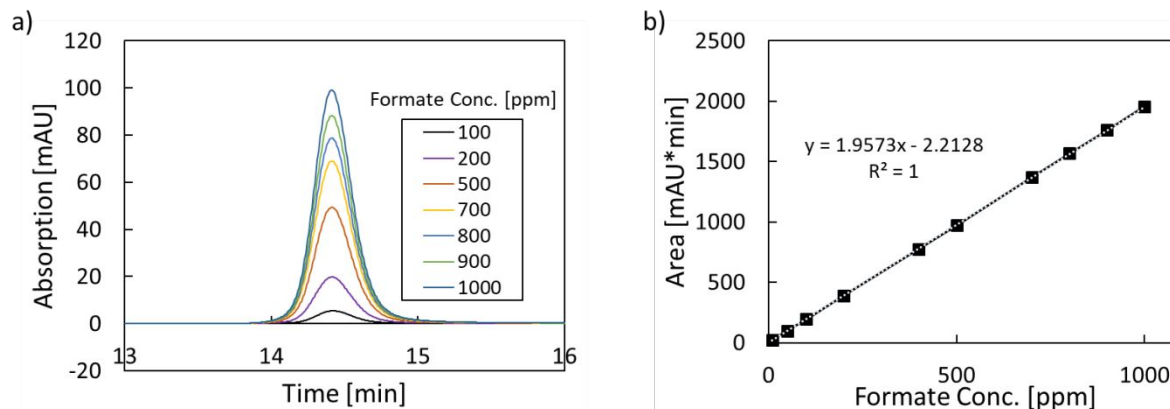


Figure S3 (a) The HPLC chromatogram of the formate standards concentration ranging from 100 ppm to 1000 ppm with retention time at 14.2 min and (b) the calibration curve of formate.

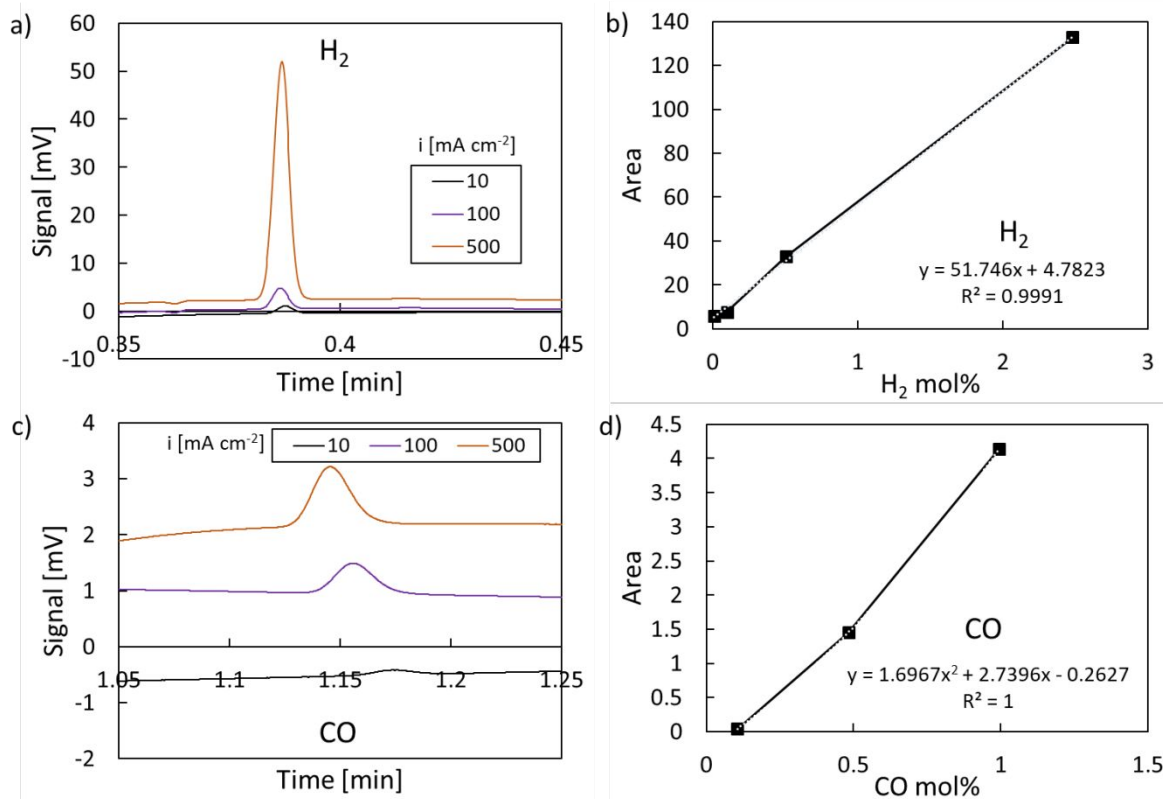


Figure S4 The examples of GC chromatogram of H₂ (a) and CO (c) at different current densities in the test of 0.75 mg_{SnO2} cm⁻². The calibration curves of H₂ (b) and CO (d).

Faradaic Efficiency (FE) Calculations

The FE of formate in the liquid samples is calculated from equation S1. The analyte in the liquid samples being measured in HPLC is formic acid instead of formate salt due to the pKa of formic acid being 3.77 and the pH of the mobile phase (4 mM H₂SO₄) being ~1.3. For gas samples, the FE is calculated by equation S2. Composition on a mole percentage basis are returned from GC. The gas samples were treated as ideal gas and integrating the measured flow rate yields mole of gas analytes.

$$FE_i = \frac{n_i * F * C_i * V}{j * A * t} \quad (S1)$$

$$FE_i = \frac{n_i * F}{j * A * t} * \frac{P * x_i}{R * T_l} * \int V_g(t) dt \quad (S2)$$

Where:

n_i : number of required electrons

F: Faraday's constant

C_i : analyte concentration

V_t : volume of the collected sample

j: current density

A: geometric area of electrode (25 cm² in this study)

t: sampling time

V_g : gas flow rate

P: absolute pressure

x_i : mol% of the analyte gas

T_l : temperature of the sampling loop

Nano-CT Imaging of the Catalyst Layer

Following the procedure described in the work of Cetinbas et al.,⁶ X-ray radiographs were acquired using the Xradia nano XCT-S100 TXM at beamline 32-ID-C at the Advanced Photon Source, Argonne National Laboratory. At 8-keV energy level with 0.5 s X-ray exposure time, 1080 images were recorded over 180° rotation. Using a Fresnel zone plate with 60-nm outermost zone

width, the X-ray images are taken in Zernike phase contrast mode. This mode provides contrast relying on determination of the phase shift of the transmitted X-rays and allows imaging low electron density materials (i.e. C). The projection images are reconstructed into three-dimensional data set with 20-nm voxel resolution using the software Tomopy⁷ and Astra⁸. At this resolution, field of view (FOV) at 32-ID-C is limited to 50- μm diameter and 50- μm tall cylinder. In order to keep the samples in the FOV, the tip of the sharp-pointed-triangle-cuts from GDEs were scanned. Figure S5 shows a section of the reconstructed data together with the segmented image indicating the electrode material in blue color and pore space in black.

Reconstructed phase contrast data

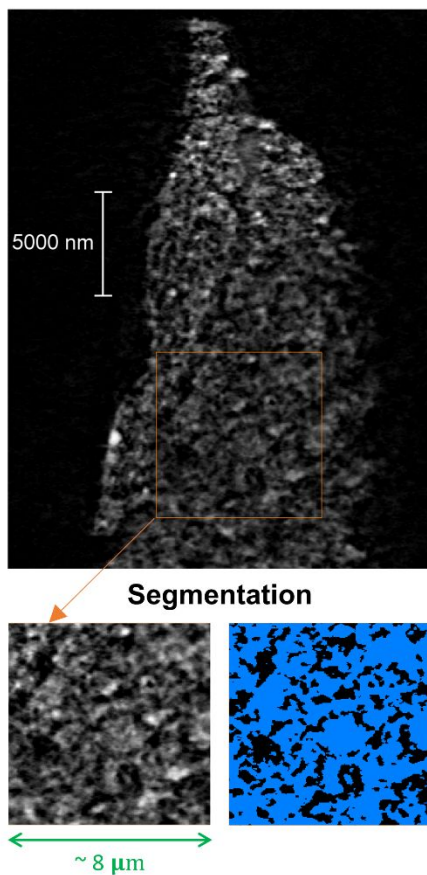


Figure S5. A section showing the reconstructed phase contrast data and segmentation.

Scanning Electron Microscope (SEM) Imaging of the Cathode GDE

The surface and cross-section morphological characterization of the catalyst layer on cathode GDE was performed using a Hitachi S-4800 SEM.

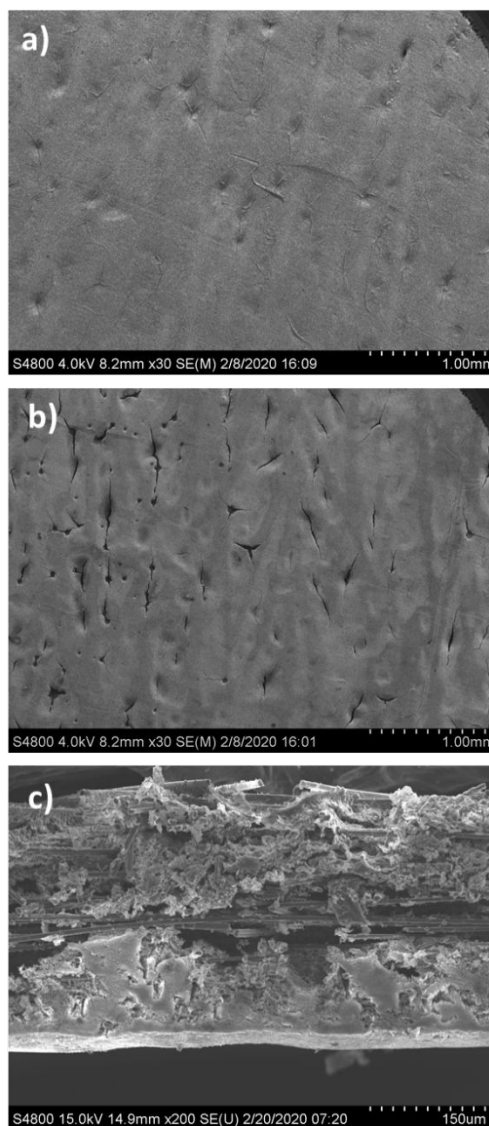


Figure S6 Top-down images of the catalyst layer of 0.5 mg cm⁻² SnO₂ loading on the GDE before (a) and after (b) the test. The cross-section of a 1.5 mg cm⁻² cathode GDE, with the bottom layer showing as the catalyst layer (c).

BPM Characterization in a Flow Cell

The BPM was characterized in a tailor-made four-chamber (anode rinse, base, acid, and cathode rinse) flow cell shown in Figure S7. A 1 M NaOH solution was fed to the anode rinse chamber and base chamber at 10 mL min^{-1} , and 1 M H_2SO_4 was fed to the cathode rinse chamber and 0.4 M K_2SO_4 to acid chamber at 10 mL min^{-1} . Two pieces of Pt foil (99.99%, 0.001 inch thick, Alfa Aesar) supported on Ti plates were used as the working and counter electrodes. The BPM was placed at the center of the cell with an AEM (Neosepta AHA) and a CEM (Nafion NR-212) at each side to minimize the influence of the electrode reaction on measurements. The effective BPM area was defined using a 1.2-cm-diameter circular aperture. The potential difference across the membrane was measured by a $\text{Hg}/\text{Hg}_2\text{SO}_4$ reference electrode (filled with saturated K_2SO_4 , $E^0 = 0.64 \text{ V vs. NHE at } 25^\circ\text{C}$) in the acidic chamber and a Hg/HgO reference electrode (filled with 1 M NaOH, $E^0 = 0.098 \text{ V vs. NHE at } 25^\circ\text{C}$) in the alkaline chamber. Chronopotentiometry and galvanostatic electrochemical impedance spectroscopy (EIS) of BPMs were conducted at room temperature using a Gamry Reference 3000 potentiostat in a standard four-electrode setup. In EIS measurements, an AC amplitude of 10% of the applied DC current and a frequency spectrum from 300 kHz to 1 Hz was employed.

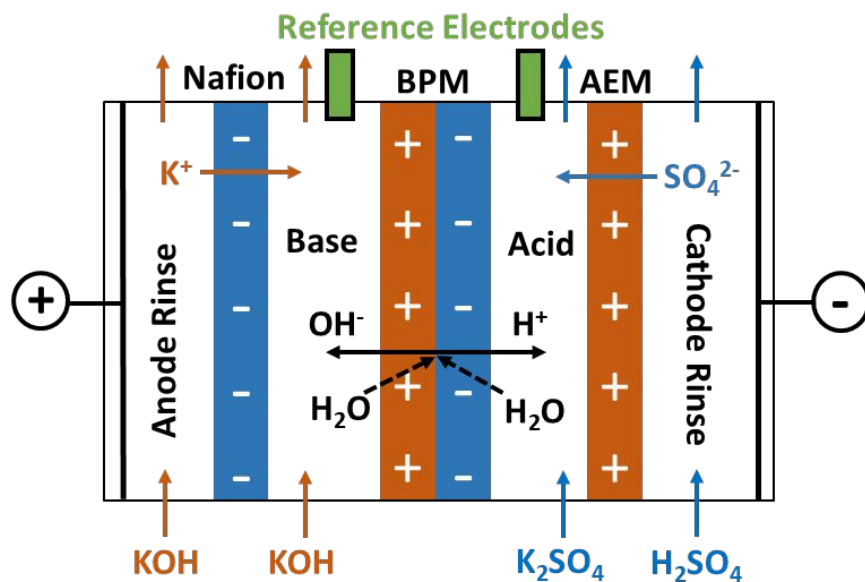


Figure S7 Schematic diagram of the flow cell for BPM characterization.

Voltage Breakdown using Gold Wire

The use of a gold wire as a pseudo-micro reference electrode was initially reported by Buchi⁹ where it served the same purpose as a Luggin capillary in PEM FCs. In addition, gold wires have also been used in lithium ion batteries as a micro-reference electrode¹⁰ where they showed stable and accurate impedance and potential measurements. In this study, the gold wire provides reliable potential drop measurements without sacrificing the cell performance from extra ohmic losses from the electrolyte layer (Figure S8).

The stability of the measurements by the gold ribbon wire is validated in Figure S7. The potential drop from the gold wire to cathode current collector measured from galvanodynamic scan at $1 \text{ mA cm}^{-2} \text{ s}^{-1}$ matches well with that measured from holding at each current density.

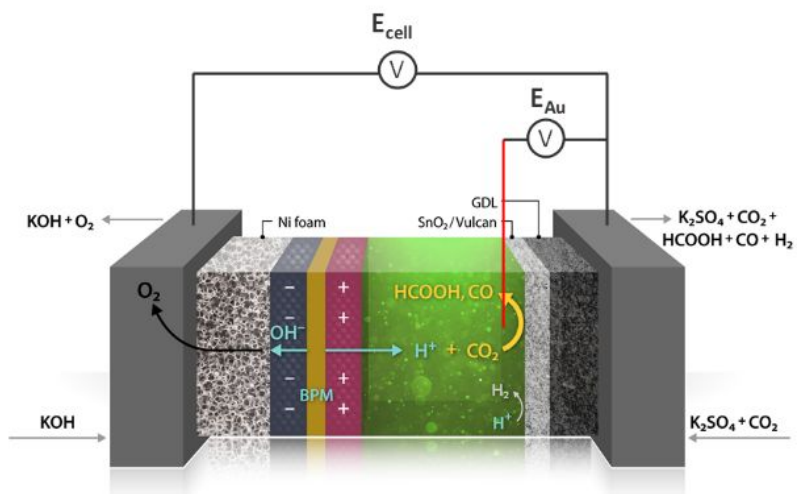


Figure S8 The whole-voltage and the voltage drop between the gold wire and cathode current collector measurement.

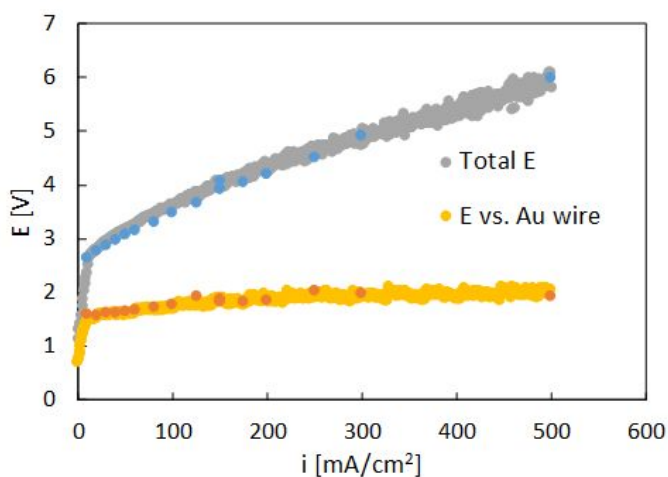
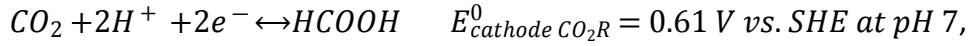


Figure S9 The whole-voltage and the voltage drop between the gold wire and cathode current collector measured from galvanodynamic scan and galvanostatic current holding overlaps well.

The gold ribbon wire was 127 μm distance from the cathode GDE, while the whole liquid electrolyte layer was 1270 μm thickness. Therefore, the measured voltage obtained from the LabJack is defined as

$$E_{Au} = \frac{1}{10}IR_{Electrolyte} + E_{Cathode CO_2R}^0 + \eta_{Cathode CO_2R}$$

where $R_{Electrolyte} = 0.078 \Omega$ was calculated from the conductivity of 0.4 M K_2SO_4 of 65.14 mS cm^{-1} , $E_{Cathode CO_2R}^0$ is the thermodynamic potential of CO_2R



and $\eta_{Cathode CO_2R}$ is the overpotential of CO_2R .

The potential drop between the anode current collector and the gold wire is determined as

$$E_{cell} - E_{Au} = \frac{9}{10}IR_{Electrolyte} + E_{BPM Junction} + E_{BPM IEL} + E_{Anode OER}^0 + \eta_{Anode OER}$$

Where $E_{BPM Junction}$ is the water dissociation potential at the junction of BPM, $E_{BPM IEL}$ is the voltage loss from the ion exchange layers of the BPM, $E_{Anode OER}^0$ is the thermodynamic potential of OER at anode



and $\eta_{Anode OER}$ is the overpotential of OER.

The electrochemical properties of BPM were characterized by the impedance measurements in the flow cell. The same electrolyte used in the CO_2R electrolyzer – 1 M KOH next to AEL and 0.4 M K_2SO_4 next to CEL – was used in the flow cell in order to capture the properties of the BPM under the same condition.

The electronic resistance of the cell is too small to be considered here¹¹.

Reference Test using Bare GDL

In order to make sure that the formate FE in this study is contributed from the SnO₂ catalyst layer on the GDEs, instead of from the carbon paper GDL, a reference test with a bare GDL was performed in the same device at the exact same testing conditions. Formate and H₂ are the only two products found in this test. With only <4% FE of formate produced, it is confident to say that in our CO₂R test with SnO₂, the majority of CO₂R FE came from the SnO₂ catalyst layer, instead of the carbon paper.

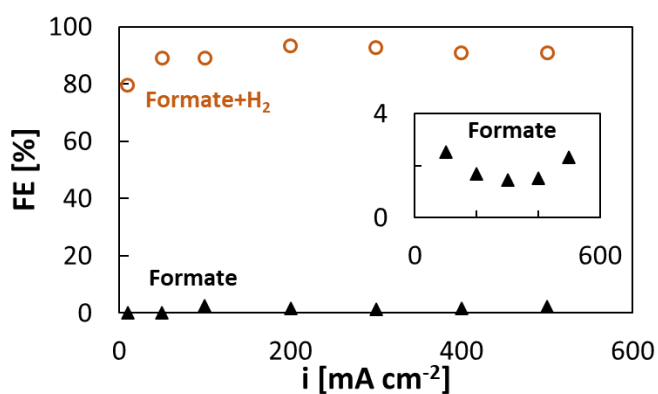


Figure S10 The formate FE and the sum of formate and H₂ FE vs. current density from the reference test with bare GDL 39BC.

References

- (1) Park, A. M.; Owczarczyk, Z. R.; Garner, L. E.; Yang-Neyerlin, A. C.; Long, H.; Antunes, C. M.; Sturgeon, M. R.; Lindell, M. J.; Hamrock, S. J.; Yandrasits, M.; et al. Synthesis and Characterization of Perfluorinated Anion Exchange Membranes. *ECS Trans.* **2017**, *80* (8), 957–966. <https://doi.org/10.1149/08008.0957ecst>.
- (2) Smith, R. D. L.; Prévot, M. S.; Fagan, R. D.; Zhang, Z.; Sedach, P. A.; Siu, M. K. J.; Trudel, S.; Berlinguette, C. P. Photochemical Route for Accessing Amorphous Metal Oxide Materials for Water Oxidation Catalysis. *Science*. **2013**, *340* (6128), 60–63. <https://doi.org/10.1126/science.1233638>.
- (3) Trotochaud, L.; Young, S. L.; Ranney, J. K.; Boettcher, S. W. Nickel-Iron Oxyhydroxide Oxygen-Evolution Electrocatalysts: The Role of Intentional and Incidental Iron Incorporation. *J. Am. Chem. Soc.* **2014**, *136* (18), 6744–6753. <https://doi.org/10.1021/ja502379c>.
- (4) Salvatore, D. A.; Weekes, D. M.; He, J.; Dettelbach, K. E.; Li, Y. C.; Mallouk, T. E.; Berlinguette, C. P. Electrolysis of Gaseous CO₂ to CO in a Flow Cell with a Bipolar Membrane. *ACS Energy Lett.* **2018**, *3* (1), 149–154. <https://doi.org/10.1021/acseenergylett.7b01017>.
- (5) Kemperman, A. J. . *Handbook Bipolar Membrane Technology*; Twente University Press: Enschede, 2000.
- (6) Cetinbas, F. C.; Ahluwalia, R. K.; Kariuki, N.; De Andrade, V.; Fongalland, D.; Smith, L.; Sharman, J.; Ferreira, P.; Rasouli, S.; Myers, D. J. Hybrid Approach Combining Multiple

- Characterization Techniques and Simulations for Microstructural Analysis of Proton Exchange Membrane Fuel Cell Electrodes. *J. Power Sources* **2017**, *344*, 62–73. <https://doi.org/10.1016/j.jpowsour.2017.01.104>.
- (7) Pelt, D. M.; Gürsoy, D.; Palenstijn, W. J.; Sijbers, J.; De Carlo, F.; Batenburg, K. J. Integration of TomoPy and the ASTRA Toolbox for Advanced Processing and Reconstruction of Tomographic Synchrotron Data. *J. Synchrotron Radiat.* **2016**, *23* (3), 842–849. <https://doi.org/10.1107/S1600577516005658>.
- (8) De Andrade, V.; Deriy, A.; Wojcik, M. J.; Ursoy, D. G. ; Shu, D.; Fezzaa, K.; De Carlo, F. Nanoscale 3D Imaging at the Advanced Photon Source. *SPIE Newsroom* **2016**. *10* (2), 1201604. <https://doi.org/10.1117/2.1201604.006461>.
- (9) Büchi, F. N.; Scherer, G. G. In-Plane Resolved In-Situ Measurements of the Membrane Resistance in PEFCs . *ECS Proc. Vol.* **1998**, *1998–27*, 71–80. <https://doi.org/10.1149/199827.0071pv>.
- (10) Solchenbach, S.; Pritzl, D.; Kong, E. J. Y.; Landesfeind, J.; Gasteiger, H. A. A Gold Micro-Reference Electrode for Impedance and Potential Measurements in Lithium Ion Batteries. *J. Electrochem. Soc.* **2016**, *163* (10), A2265–A2272. <https://doi.org/10.1149/2.0581610jes>.
- (11) Neyerlin, K. C.; Gu, W.; Jorne, J.; Gasteiger, H. A. Study of the Exchange Current Density for the Hydrogen Oxidation and Evolution Reactions. *J. Electrochem. Soc.* **2007**, *154* (7), B631. <https://doi.org/10.1149/1.2733987>.